Dislocation density evaluation of three commercial SA508Gr.3 steels for reactor pressure vessel

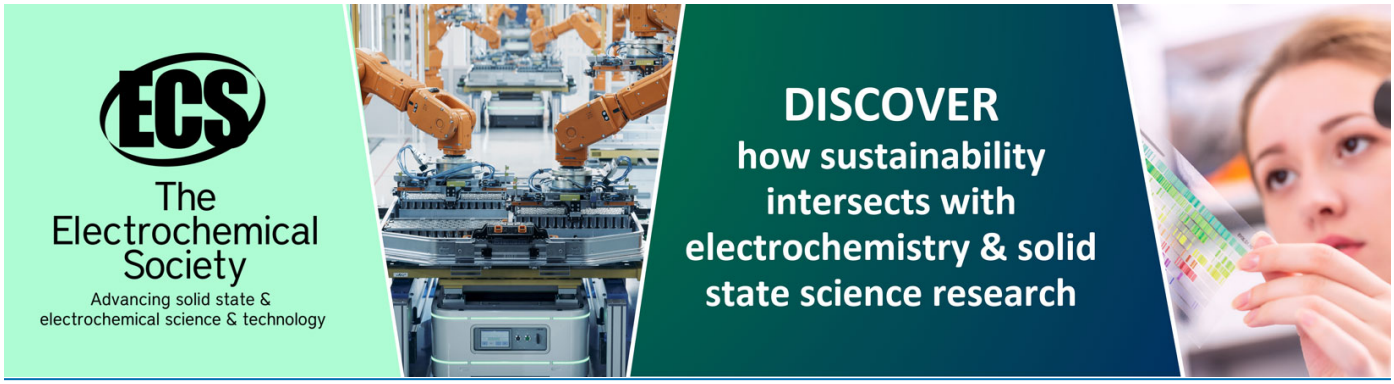

Dislocation density evaluation of three commercial SA508Gr.3 steels for reactor pressure vessel

Hailong Liu[1, 2] and Qiulin Li[2,*]

[1]School of Material Science and Engineering, Tsinghua University, Beijing, China
[2]Graduate School at Shenzhen, Tsinghua University, Shenzhen, China

*Corresponding author e-mail: liql@sz.tsinghua.edu.cn

Abstract. Reactor pressure vessel (RPV) plays a crucial role in the safe operation of nuclear power plants (NPPs). However, RPV steels are generally subjected to high-energy neutron irradiation during the entire in-service lifetime, which causes the hardening and embrittlement of RPV steels. The dislocation density (ρ) is known to affect strongly the mechanical properties of RPV steels. The dislocation density of three commercial SA508 Gr.3 steels manufactured by different countries was thoroughly investigated by X-ray diffraction (XRD), electron backscattered diffraction (EBSD) and transmission electron microscopy (TEM). The dislocation densities of three SA508 Gr.3 steels calculated by XRD are as high as 10^{13} m^{-2} and consistent with results of tempered steels reported in prior studies. The results calculated by XRD match qualitatively with those obtained from TEM and kernel average misorientation (KAM) analysis of EBSD (EBSD-KAM).

1. Introduction

RPV steel is one of the most crucial structural materials used for the nuclear reactors because of serving as a barrier for pressure and radioactive fission products produced during the nuclear fission reaction [1-3]. However, the irradiation embrittlement and hardening of RPV are known to threaten the safe operation of nuclear power plants (NPPs). Many investigations have been performed to explore the mechanism of the embrittlement and hardening of RPV steels. The degradation of mechanical properties of RPV steels induced neutron irradiation is generally ascribed to three kinds of microstructural changes: (i) nanoscale solute clusters or precipitates, (ii) matrix damage and (iii) P segregation at grain boundaries [4-6]. The prior investigations confirmed that irradiation damage is strongly influenced by microstructural parameters, including dislocations and grain boundaries [7, 8]. As a key microstructural defect in materials, dislocation density indirectly affects the mechanical and physical properties of metals and alloys. The stored energy provided by a high dislocation density is the driving force for nucleation of solute clusters or precipitates [9-11]. The high dislocation density might accelerate the formation of solute-rich clusters that cause the embrittlement of RPV steels. However, high dislocation density can supply more sinks for point defects (PDs) to improve irradiation tolerance [12]. Therefore, a quantitative evaluation for the dislocation density of RPV steels is necessary to explore the mechanism of interaction between dislocations and irradiation damage.

The XRD, TEM and EBSD are three kinds of most common and useful techniques to investigate the dislocation density in metal. However, different methods are suitable for different dislocation densities. For instance, TEM and EBSD are less advisable for severely deformed metals where dislocations density is too high to make an accurate statistical analysis for individual dislocations. The

XRD method is more reliable because peak broadening caused dislocations is very large. Some researchers have conducted many investigations on dislocation density of tempered steel by the combination of XRD and TEM. The corresponding results showed that the tempered martensitic or bainitic steels had a high dislocation density from 10^{13} to 10^{14} m^{-2} [13-17]. Severely deformed Fe-based materials have a dislocation-density value of 10^{15} m^{-2}, for example, 80% cold rolling ODS-Eurofer steel [18]. This work aims to evaluate and compare the dislocation density of three commercial RPV steels. In this study, the dislocation density of three commercial RPV steels was investigated by the combination of different characterization techniques, such as XRD, TEM and KAM. Moreover, there are a large number of experimental data on the dislocation density of the low alloy steels in prior literatures, allowing a direct comparison between different kinds of commercial RPV steels.

2. Materials and Methods

2.1. Materials

The materials in this study are three commercial SA 508 Gr.3 steels supplied by China Nuclear Power Engineering Co., Ltd. (CNPDC). In this study, three kinds of SA 508 Gr.3 steels are abbreviated as A, B and C-RPV, respectively. Table 1 and 2 show the chemical composition and mechanical properties of these RPV steels, respectively. Three SA 508 Gr.3 steels have similar chemical compositions, but slightly different mechanical properties probably due to the differences in manufacturing processes, shown in Table 1 and 2.

Table 1. The chemical composition (wt.%) of three commercial RPV steels in this study.

RPV Steels	Element (wt.%)									
	C	Si	Mo	S	Cu	P	Cr	Mn	Ni	Fe
A-RPV	0.18	0.22	0.47	0.001	0.029	0.004	0.12	1.37	0.74	Bal.
B-RPV	0.18	0.18	0.48	0.001	0.013	0.004	0.12	1.43	0.73	Bal.
C-RPV	0.18	0.18	0.50	0.001	0.025	0.004	0.11	1.35	0.73	Bal.

Table 2. The high temperature (350°C) and room temperature (RT) tensile properties of three commercial RPV steels in this study.

RPV steels	Temperature /°C	Yield strength /MPa	Tensile strength /MPa	Percentage elongation /%	Percentage reduction of area /%
A-RPV	RT	445	584	≥20	-
	350	383	548	-	-
B-RPV	RT	494	629	27	74
	350	430	588	24	76
C-RPV	RT	442	587	27.5	77
	350	383	554	27.8	76.5

2.2. Experimental Methods

The X-ray diffraction profiles were measured by the Rigaku D/Max 2500/PC diffractometer, which is operated at 40 KV and 200 mA and equipped with $Cu_{k\alpha}$ radiation and a silicon array detector. Each sample was ground by abrasive papers, followed by mechanical and electrochemical polishing to remove surface damage. The diffraction profiles with a range from 2θ=40° to 120°were recorded in two steps: Firstly, each sample was rapidly scanned with a 0.02° step and 0.3 s counting time. Secondly, each diffraction peak of diffraction profile was precisely scanned with a 0.01° step and 4.8 s counting time. Five diffraction peaks were used for estimating the dislocation density in this study. Proprietary software made in Tsinghua University was used to eliminate the $K_{\alpha 2}$ radiation and instrumental line broadening. The diffraction profiles corresponding to $K_{\alpha 1}$ radiation were fitted with Pseudo-Voigt function and used for later analysis.

The microstructural characterization was performed using a Tescan Mira 3LMH field emission scanning electron microscopy (SEM) equipped with an HKL Nordly Max EBSD detector produced by

the Oxford Instruments Company. The EBSD maps of all samples were obtained with a step of 100 nm, and the HKL Channel 5 software was used for the KAM analysis. The 3 mm diameter disks were cut from 100 μm thick RPV steel sheets. The 3 mm disks were ground further down to 50 μm and finally thinned into TEM foils with electron transparency using a double-jet electrolytic polishing in an electrolyte of 90 % acetic acid and 10 % perchloric acid at 253 K. The dislocation observation of three RPV steels was performed using a TEM JEOL JEM-2100 operated at 200 kV.

3. Results and discussion

3.1. The evaluation of dislocation density by XRD

Many literatures reported that the X-ray diffraction peak broadening is caused by two microstructural factors: (i) the size broadening, independent of diffraction order; (ii) the strain broadening, which increases as the diffraction order increases [13, 19]. Assuming strain broadening was mainly caused by dislocation, the modified Williamson-Hall (W-H) and Warren-Averbach (W-A) models are two main methods used for evaluating the dislocation density. Although W-A method is more powerful and accurate to calculate the dislocation density, the method is extremely cumbersome and error-prone. However, the W-H method is simple and feasible and has a high level of precision in analyzing the dislocation density of cubic materials [18]. Therefore, the modified W-H method was used to calculate the dislocation density of three RPV steels in this study. The modified W-H equation is shown below [20]:

$$\Delta K \cong \frac{0.9}{D} + \left(\frac{\pi M^2 b^2}{2}\right)^{\frac{1}{2}} \rho^{\frac{1}{2}} K C^{\frac{1}{2}} + O(K^2 C) \quad (1)$$

$$K = \frac{2\sin\theta}{\lambda} \quad (2)$$

$$\Delta K = \frac{2\cos\theta(\Delta\theta)}{\lambda} \quad (3)$$

Where $\Delta\theta$, θ and D are the full widths at half maximum (FWHM) of each diffraction peak, the diffraction angle and the average grain size, respectively. λ and ρ are the wavelength of X-rays (λ= 1.5406 Å) and dislocation density, respectively. b is the Burger vector of dislocations (b=0.25 nm in iron). M is a constant and C is the average contrast factors of dislocation and dislocation-like defects, respectively. The M depends on the effective outer cut-off radius of dislocations. R.A. Renzetti reported that M < 1 for annealed materials and varied between 1 and 2 for deformed materials [18]. We used M = 2 for all samples in this study. The C is calculated by the following equation for a Bragg reflection in the cubic crystal:

$$C = C_{h00}\left[1 + q\left(\frac{h^2k^2 + h^2l^2 + k^2l^2}{h^2 + k^2 + l^2}\right)\right] \quad (4)$$

Where C_{h00} is the average contrast factors of (h00) reflection according to [20]. In this study, C_{h00} = 0.285 for all samples according to [21]. The q is a parameter, which is related to the elastic constants of the crystal and the dislocation character in the samples. The W-H model provides three important microstructural features: 1) average crystallize size, D; 2) dislocation density, $\rho = 2m^2/(\pi M^2 b^2)$, m is the slope of the W-H plots; 3) dislocation character.

The modified Williamson–Hall plots for three RPV specimens are shown in Figure 1. Table 3 shows the dislocation densities of both three RPV steels calculated by the W-H model and other steels reported in prior literatures. As shown in Table 3, dislocation densities of three RPV steels reach the level of 10^{13} m^{-2}, which are in good agreement with results reported in prior literatures. The dislocation density of the A-RPV steels is just 1.8×10^{14} m^{-2}, apparently lower than those of B, C-RPV steel (3.1×10^{14} and 2.6×10^{14} m^{-2}, respectively).

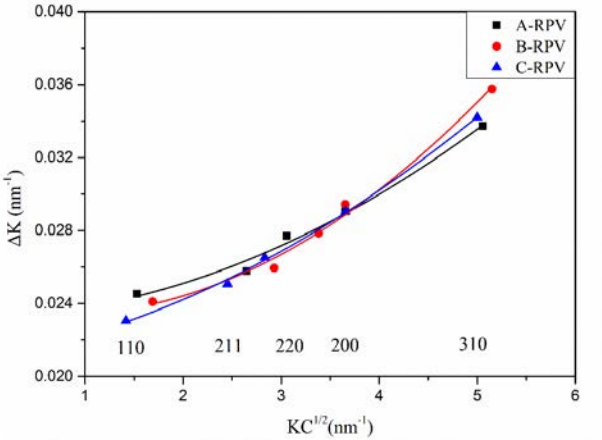

Figure 1. The modified W-H plots for three commercial RPV steel. The Miller indices of each reflection are shown in the figure.

Table 3. The dislocation densities of three RPV steels in this work and other steels reported in prior literatures.

Material	Microstructure	Heat treatment	ρ_{TEM} / $10^{14}m^{-2}$	ρ_{XRD} / $10^{14}m^{-2}$	Ref.
A-RPV	Tempered	-	-	0.18	-
B-RPV	Tempered	-	-	0.31	-
C-RPV	Tempered	-	-	0.26	-
X20-3	Tempered	750°C , 1h	0.98±0.27	0.86	[13]
X20-5	Crept	650°C, 120MPa, 1.2%	0.30±0.36	0.14	[13]
X20-6	Crept	650°C, 120MPa, 8%	0.29±0.36	0.14	[13]
P91-1	tempered	750°C, 0.25h	-	0.79	[13]
P91-3	Tempered	750°C, 1h	-	0.60	[13]
P91-4	tempered	750°C, 1h	-	0.06	[13]
12%Cr TMFS	Martensite	Initial	1.02	-	[22]
12%Cr TMFS	Tempered	550°C, 12456h	0.49	-	[22]
ODS steel	Tempered	750°C, 2h	-	2	[18]
9Cr-1W	Tempered	-	-	0.1-1[a]	[23]

[a] This data is not calculated by XRD. A detail description of the calculation method is found in [23].
- No data.

3.2. TEM & KAM analysis of dislocation density

To confirm the validity of the XRD results, TEM and KAM are also used for evaluating the dislocation density of three RPV steels in this study. The XRD methods can indirectly yield average dislocation density but not accounting for microstructure heterogeneity. However, TEM is suitable for straightforwardly observing the dislocation distribution but not providing insufficient statistics, especially for bainitic steel due to the limitation of operational area and microstructure heterogeneity. Therefore, TEM is applied for a qualitative analysis instead of a quantitative analysis in this study. Figure 2 is the TEM bright micrographs for A-RPV, B-RPV and C-RPV steels respectively. From these TEM micrographs, predominant microstructures of three SA508 Gr.3 steels are tempered bainitic, which is consistent with the results reported in the prior studies [1, 24-26]. The tempered bainitic microstructure has a striking feature, that is, there are areas containing dislocations while others are free of dislocations. Moreover, the high angle grain boundaries (HAGBs) are mainly decorated with numerous coarse carbides, and fine, spherical or needle carbides are dispersed inside the laths with a high number density. Figure 2(a) shows that there are almost no dislocations in the A-RPV specimens. Note that a large number of dislocations is observed in the B-RPV specimens, shown in Figure 2(b).

Figure 2(c) shows that the dislocation density for C-RPV steels is higher than that of A-RPV, but lower than that of B-RPV. These results match well with XRD results, which confirms the validation of XRD used for evaluating dislocation density. As an example, the areas containing dislocation are marked with yellow circles or arrows, but carbides are marked with red arrows in Figure 2.

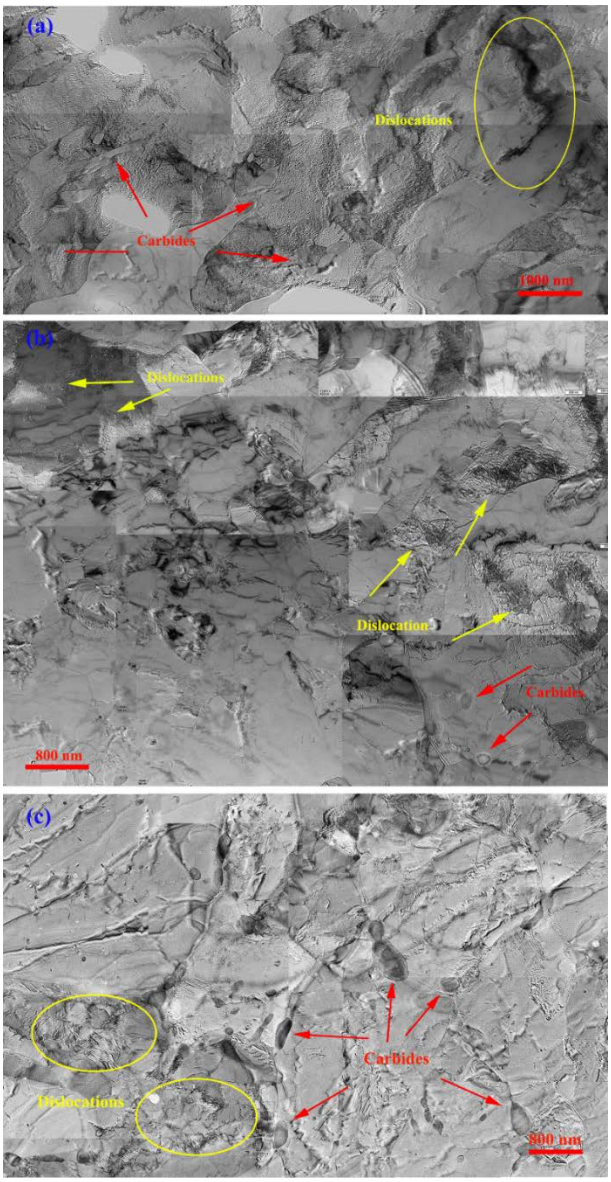

Figure 2. The bright field TEM (BF-TEM) maps of the as-received A, B and C-RPV steel.

The KAM is a powerful method to evaluate the local plastic strain gradients of materials [26]. The KAM represents the average misorientation between a given pixel and the nearest neighbors with misorientation lower than 5°, which are considered to belong to the same grain. Generally, KAM is dependent on the geometrical necessary dislocations (GNDs) density [27, 28]. In this study, KAM is used to statistically analyze the misorientation under 5° and show the differences of geometrical necessary dislocations (GNDs) density inside the grains. Figure 3 is the KAM maps of A-RPV, B-RPV, C-RPV, and their corresponding frequency distribution. The average values of KAM are 0.880, 0.954 and 0.901 in the A, B and C-RPV specimens, respectively. The KAM is known to reflect the density of GNDs in metal. The GNDs in the B-RPV steels are the highest in number density among three RPV steels due to a high average KAM value, which is in agreement with results of XRD and

TEM. However, noted that some grains, whose KAM is almost zero, are observed in three kinds of specimens, especially for A-RPV, which are probably ascribed to the occurrence of recrystallization during the manufacturing processes. The results of KAM and TEM confirmed the validation of XRD measurement in terms of dislocation density evaluation for bainitic steels.

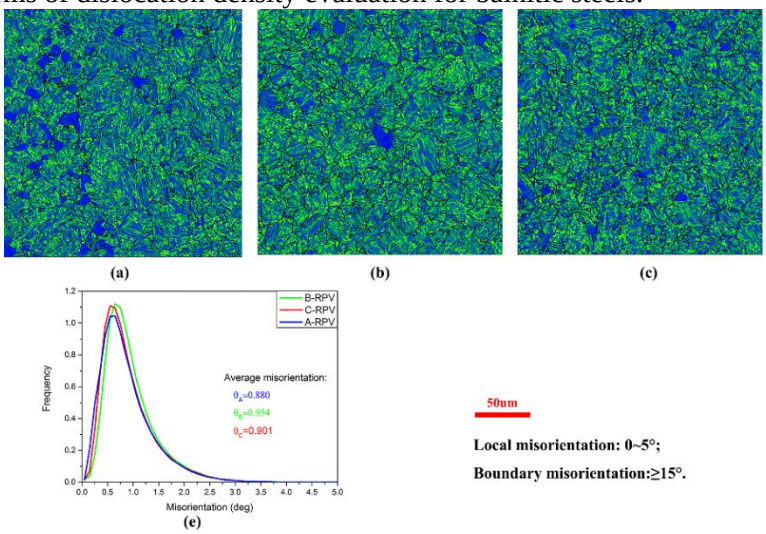

Figure 3. The KAM maps of (a) A-RPV, (b) B-RPV and (c) C-RPV; (e) the frequency distribution of KAM for three commercial RPV specimens.

4. Conclusion

The dislocation density of three commercial SA508 Gr.3 steels was evaluated by using XRD, TEM and EBSD-KAM. The dislocation densities of three SA508 Gr.3 steels obtained from the modified W-H models are as high as 10^{13} m^{-2}, and consistent with results of tempered steels reported in prior studies. Dislocation density is the lowest for A-RPV steels and highest for B-RPV steels in three SA508 Gr.3 steels. Nevertheless, the results of dislocation density obtained by XRD match qualitatively with those provided by KAM and TEM.

Acknowledgments

This study was supported by the National Key Research and Development Program under Grant No.: 2017YFB0305304; the Shenzhen Science and Technology R & D Funds under Grant No.: JCYJ20170307153239266; and China Nuclear Power Engineering Co., Ltd. under Grant No.: 2013966003).

References

[1] G.R. Odette, G.E. Lucas, Embrittlement of nuclear reactor pressure vessels, Jom 53(7) (2001) 18-22.
[2] S.J. Zinkle, G.S. Was, Materials challenges in nuclear energy, Acta Mater. 61(3) (2013) 735-758.
[3] W.L. Server, T.C. Hardin, J. Brian Hall, U.S. High Fluence Power Reactor Surveillance Data—Past and Future, J. Press. Vess. T. 136(2) (2014) 021603.
[4] R.G. Carter, N. Soneda, K. Dohi, Microstructural characterization of irradiation-induced Cu-enriched clusters in reactor pressure vessel steels, J. Nucl. Mater. 298(3) (2001) 211-224.
[5] J. Kočík, E. Keilová, J. Čížek, I. Procházka, TEM and PAS study of neutron irradiated VVER-type RPV steels, J. Nucl. Mater. 303(1) (2002) 52-64.
[6] K. Fujii, K. Fukuya, N. Nakata, Hardening and microstructural evolution in A533B steels under high-dose electron irradiation, J. Nucl. Mater. 340(2-3) (2005) 247-258.
[7] X.M. Bai, A.F. Voter, R.G. Hoagland, Efficient annealing of radiation damage near grain boundaries via interstitial emission, Sci. 327(5973) (2010) 1631-4.
[8] Z. Chang, Multiscale modelling of radiation-enhanced diffusion phenomena in metals, Stockholm: KTH Royal Institute of Technology, 2015, pp. 21-39.

[9] T. Onitsuka, M. Takenaka, E. Kuramoto, Deformation-enhanced Cu precipitation in Fe-Cu alloy studied by positron annihilation spectroscopy, Phys. Rev. B 65(1) (2001).
[10] R. Rana, S.B. Singh, O.N. Mohanty, Effect of composition and pre-deformation on age hardening response in a copper-containing interstitial free steel, Mater. Charact. 59(7) (2008) 969-974.
[11] Y. Kamada, S. Takahashi, H. Kikuchi, Effect of pre-deformation on the precipitation process and magnetic properties of Fe–Cu model alloys, J. Mater. Sci. 44(4) (2009) 949-953.
[12] Z. Chang, D. Terentyev, N. Sandberg, Anomalous bias factors of dislocations in bcc iron, J. Nucl. Mater. 461 (2015) 221-229.
[13] J. Pešička, R. Kužel, A. Dronhofer, The evolution of dislocation density during heat treatment and creep of tempered martensite ferritic steels, Acta Mater. 51(16) (2003) 4847-4862.
[14] P.J. Ennis, A. Zielinska-Lipiec, O. Wachter, Microstructural stability and creep rupture strength of the martensitic steel P92 for advanced power plant, Acta Mater. 45(12) (1997) 4901-4907.
[15] J. Peŝiĉka, A. Dronhofer, G. Eggeler, Free dislocations and boundary dislocations in tempered martensite ferritic steels, Mater. Sci. Eng., A 387-389 (2004) 176-180.
[16] C.G. Panait, A. Zielińska-Lipiec, T. Koziel, Evolution of dislocation density, size of subgrains and MX-type precipitates in a P91 steel during creep and during thermal ageing at 600C for more than 100,000h, Mater. Sci. Eng., A 527(16-17) (2010) 4062-4069.
[17] S. Takebayashi, T. Kunieda, N. Yoshinaga, Comparison of the Dislocation Density in Martensitic Steels Evaluated by Some X-ray Diffraction Methods, ISIJ Int. 50(6) (2010) 875-882.
[18] R.A. Renzetti, H.R.Z. Sandim, R.E. Bolmaro, X-ray evaluation of dislocation density in ODS-Eurofer steel, Mater. Sci. Eng., A 534 (2012) 142-146.
[19] T. Ungár, Microstructural parameters from X-ray diffraction peak broadening, Scripta Mater. 51(8) (2004) 777-781.
[20] T. Ungár, G. Tichy, The Effect of Dislocation Contrast on X-Ray Line Profiles in Untextured Polycrystals, Phys. Status Solidi A 171(2) (1999) 425-434.
[21] T. Ungár, I. Dragomir, Á. Révész, The contrast factors of dislocations in cubic crystals: the dislocation model of strain anisotropy in practice, J. Appl. Crystallogr. 32(5) (1999) 992-1002.
[22] J. Pešička, A. Aghajani, C. Somsen, How dislocation substructures evolve during long-term creep of a 12% Cr tempered martensitic ferritic steel, Scripta Mater. 62(6) (2010) 353-356.
[23] M. Tamura, F. Abe, Changes in Estimated Dislocation Density during Creep in Martensitic Heat-Resistant Steel, J. Mater. Sci. Res. 4(4) (2015).
[24] W.-J. Yang, B.-S. Lee, Y.-J. Oh, Microstructural parameters governing cleavage fracture behaviors in the ductile–brittle transition region in reactor pressure vessel steels, Mater. Sci. Eng., A 379(1-2) (2004) 17-26.
[25] M. Karlík, I. Nedbal, J. Siegl, Microstructure of a reactor pressure vessel steel close to the zones of ductile tearing and cleavage, Mater. Sci. Eng., A 357(1-2) (2003) 423-428.
[26] S. Lee, S. Kim, B. Hwang, Effect of carbide distribution on the fracture toughness in the transition temperature region of an SA 508 steel, Acta Mater. 50(19) (2002) 4755-4762.
[27] S.I. Wright, M.M. Nowell, D.P. Field, A review of strain analysis using electron backscatter diffraction, Microsc Microanal 17(3) (2011) 316-29.
[28] M. Calcagnotto, D. Ponge, E. Demir, Orientation gradients and geometrically necessary dislocations in ultrafine grained dual-phase steels studied by 2D and 3D EBSD, Mater. Sci. Eng., A 527(10-11) (2010) 2738-2746.